Research Signpost
37/661 (2), Fort P.O., Trivandrum-695 023, Kerala, India

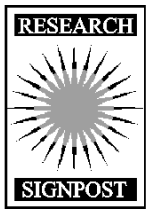

Recent Res. Devel. Optics, 7(2009): ISBN: 978-81-308-0370-8

Fractal diffractive lenses with improved diffraction efficiency

Laura Remon[1], Fernando Giménez[2], Walter D. Furlan[1], and Juan A. Monsoriu[3]
[1]Departamento de Óptica, Universitat de València, E-46100 Burjassot, Spain
[2]Departamento de Matemática Aplicada, Universidad Politécnica de Valencia E-46022 Valencia, Spain, [3]Departamento de Física Aplicada, Universidad Politécnica de Valencia, E-46022 Valencia, Spain

Abstract

In this paper we review the focusing and imaging properties of fractal photon sieves and Devil's lenses designed in order to improve the diffraction efficiency of fractal diffractive lenses. It is shown that these lenses provide a smoothing effect on the higher order foci of a conventional fractal zone plate. Furthermore, the characteristic self-similar axialesponse of the fractal zone plates is always preserved. This behavior predicts an improved performance of fractal lenses as image forming devices with an extended depth of field and a reduced chromatic aberration.

Correspondence/Reprint request: Dr. Juan A. Monsoriu Departamento de Física Aplicada, Universidad Politécnica de Valencia, E-46022 Valencia, Spain. E-mail: jmonsori@fis.upv.es

1. Introduction

Fractal zone plates (FZP) [1] where presented in 2003 as curious diffractive elements with many potential applications in several scientific and technological areas. These elements are essential in image forming setups that are used in THz tomography, soft X-ray microscopy, astronomy, and lithography. The main property of a FZP is its fractal structure along the squared radial coordinate. It has been shown that FZPs have multiple foci replicating its fractality internally at each focus along the optical axis [2-4].

In this text we show two different mechanisms to control the diffraction efficiency of this kind of fractal lenses have been proposed in order to design realistic optical systems. The diffraction efficiency of a FZP can be controlled by amplitude modulation, resulting in new elements called fractal photon sieves (FPS) [5,6] and also by certain pure phase FZPs known as *Devil's lenses* (DLs) [7].

A FPS developed for focusing and imaging soft X with high resolution capabilities. It consists of hundreds of small circular holes distributed over the zones of a FZP. Unlike FZP the FPS has no connected regions. This feature permits its fabrication in a single surface without any substrate. On the other hand, a DL is a kinoform element in which the surface relief is constructed using a function known as the *devil's staircase*.

In this contribution we revise the focusing properties of these two new families of diffractive elements by computing the diffraction patterns transversal to the propagation direction.

2. Fractal photon sieves

Photon sieves [8] are another new kind of diffractive optical elements, developed for focusing and imaging soft X rays with high resolution capabilities. In this section we present the design and the focusing properties of this new design.

Let us review the concept to Fresnel zone plate: As it is well known, a Fresnel zone plate consists of alternately transparent and opaque zones whose radii are proportional to the square root of the natural numbers, thus it can be generated from a 1D structure (see Fig. 1, upper part) defined by the periodic function $q(\varsigma)$, by performing a change of coordinates $\varsigma=(r_0/a)^2$ and by rotating the transformed 1-D function around one of its extremes. The result is a Fresnel zone plate having a radial coordinate r_o and an outermost ring of radius a [see Fig. 2(a)]. In a similar way a FZP is constructed by replacing the periodic function used in the generation of a Fresnel zone plate, by a 1-D fractal structure, as for example the triadic Cantor set shown in Fig. 1 (lower part). The corresponding zone plate with fractal profile is represented in Fig.

2(b). It has been shown [1-4] that the irradiance along the optical axis produced by a FZP presents multiple foci with a distinctive fractal structure. The position, size and depth of the foci depend on the fractal level and on the lacunarity of the encoded fractal structure. Based on a FZP, the FPS here proposed combines the features of FZP with the concept of photon sieve. A FPS has essentially the same structure of a FZP but instead of transparent rings the corresponding zones have been broken up into isolated circular holes. The result is shown in Fig. 2(c). In the construction procedure we adopted the results reported in Ref [8] where it has been shown that for a photon sieve constructed with a Fresnel zone plate structure, the diameter d of the holes in each ring of width w of has an optimum value for the effective contribution to the focus. This value is given by d=1.53w. As in a conventional photon sieve, the angular distribution of the holes in each ring can be fixed, or random [like in Fig. 2(c)].

As in a conventional photon sieve, the angular distribution of the holes in each ring can be fixed, or random (like en Fig. 2 (c)). In this section we show that this election is irrelevant for the axial response.

Let us consider the irradiance along the optical axis z, given by an optical system having a 2-D pupil function $p_o(r_o, \phi)$, expressed in canonical

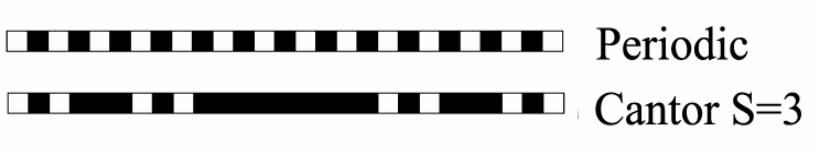

Figure 1. Periodic and fractal 1-D structures to be used to generate zone plates.

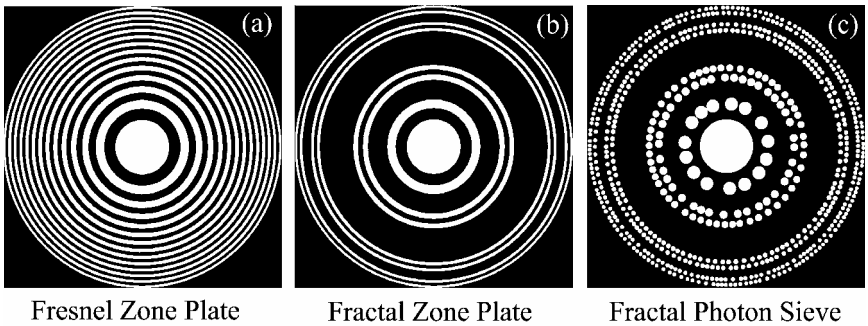

Figure 2. Comparison between (a) Fresnel zone plate, (b) FZP, and (c) FPS.

polar coordinates, when it is illuminated by a plane wave of wavelength λ:

$$I(z)=\left(\frac{2\pi}{\lambda z}\right)^2\left|\int_0^a\int_0^{2\pi} p(r_o,\phi)\,exp\left(-i\frac{\pi}{\lambda z}r_o^2\right)r_o\,d\,r_o\,d\,\phi\right|^2 \tag{1}$$

The axial irradiance in Eq. (1) can be expressed in terms of a single radial integral, by performing first the azimutal average of the pupil function $p_o(r_o, \phi)$:

$$p_o(r_o) = \frac{1}{2\pi} \int_0^a p(r_o, \phi)\, d\phi \tag{2}$$

Then Eq. (1) can be rewritten as

$$I(z) = \left(\frac{2\pi}{\lambda z}\right)^2 \left| \int_0^a p_o(r_o) \exp\left(-i \frac{\pi}{\lambda z} r_o^2\right) r_o \, d r_o \right|^2 \tag{3}$$

To compare the performance of a FPS with a conventional FZP [1] we used Eq. (2) and Eq. (3) to compare the axial irradiances provided by the corresponding pupil functions [see Figs. 2(b) and 2 (c)]. The result is show in Fig. 3. The parameters used to calculate this plots were a=2 mm, λ=632.8 nm.The number of holes in the FPS was 650 and the density of holes per zone (i.e. the ratio between the area covered by the holes and the total area of the zone) was aproximately 90%. The minimum diameter in the outermost ring was d=1.53 w=0.0572mm. The Fig (3) shows like the focal structure of a FZP along the optical axis is characterized by the coincidence of the central peak with the one obtained for a conventional Fresnel zone plate, but the internal structure of the focus reproduce the self similarity of the zone plate. This behavior is repeated at the higher-order diffraction foci [see Fig. 3(a)]. When the FZP is replaced by a FPS the principal focus remains almost unaltered but all odd higher orders are highly reduced due to the smoothing effect that the holes produce on the azimuthal average of the effective pupil [see Fig. 3(b)]. This effect is obtained at the expense of the appearance of low intensity even orders, which by design are null in the case of azimuthally uniform FZP. Note also that the secondary maxima in the principal focus are relatively higher for a FPS.

We have experimentally tested the imaging capabilities of FPS under white light illumination. For comparison images of test object (consisting of binary letters from an optotype-like chart) were formed both with a conventional Fresnel photon sieve [2] with 81 zones and with the equivalent FPS (i.e. the same diameter and same outermost pinhole diameters) constructed for S=4. The diameter of the binary zone plates used in the experiment were 5mm and their focal distances 124mm, for λ=632.8nm. The photon sieves were printed and then photographically reduced onto 35mm slides. The images of the test object were obtained directly onto an 8

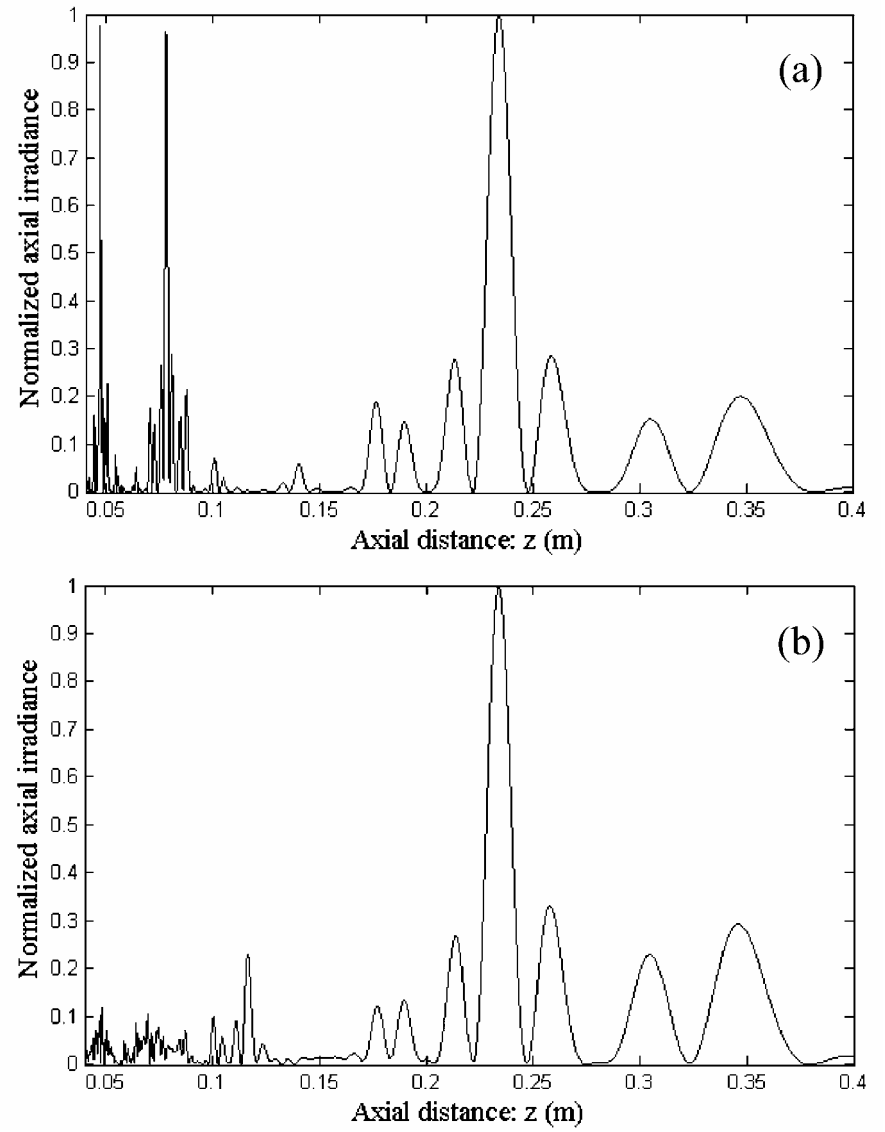

Figure 3. Normalized irradiance distributions along the optical axis produced by the lenses in Figs. 2(b) and 2(c). (a) FZP, (b) and FPS (both computed for S=3).

megapixels CMOS detector of area 22.2x14.8mm^2 (Cannon EOS 350D digital camera [3]). The results are summarized in Fig. 4. Due to the different transmittances of both kind of zone plates the range of intensities of the photographs in this figure were normalized to the peak intensity, but no additional post-processing was performed. As can be seen the out of focus image obtained with the FPS is considerably better than the one obtained with the Fresnel photon sieve (noticeable in the second and third lines of letters), the price paid to gain depth of field is a slightly poor resolution at the in-focus plane [see Figs. 4(a) and 4(b)]. Note also that the gain of the depth of field

results in a considerable reduction in chromatic aberration when using white light. In spite of being a subjective comparison the result is consistent with the prediction that can be done with the hypothesis of theoretical irradiances computed using Eq. (3). This result is shown in Fig. 5 were, for simplicity, the plots have been computed for S=3. As can be seen in Fig. 5 the reduction of the chromatic blur can be explained by the overlapping of the foci for the different wavelengths that creates an overall extended depth of field which is less sensitive to the chromatic aberration.

Next we present a modification of diffractive lenses whose structure is based on the combination of two concepts: photon sieve and fractal zone plates with variable lacunarity called Lacunar Fractal Photon Sieves (LFPS). The as a free parameter that can be used to perform apodization using a binary structure.

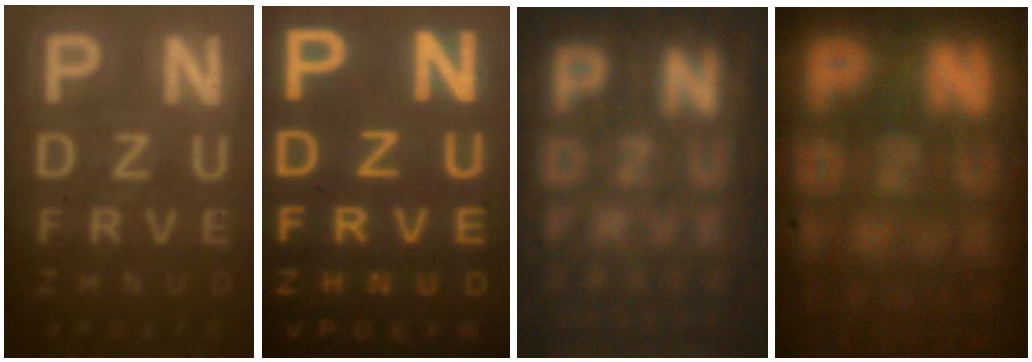

Figure 4. (a) Image obtained with FPS in the green focus. (b) Image obtained with Fresnel photon sieve in the green focus. (c) Image obtained with FPS in the defocused toward the object.(d) Image obtained with Fresnel photon sieve in the defocused toward the object.

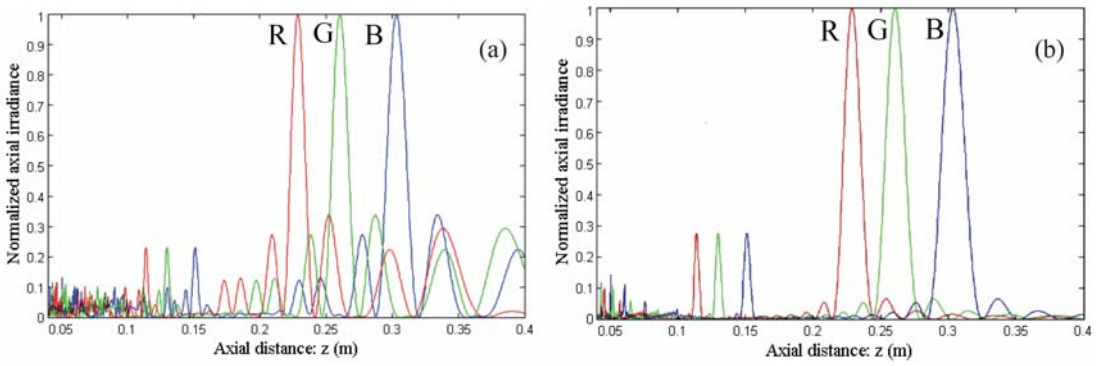

Figure 5. Axial irradiances computed for (a) the Fresnel photon sieve and (b) the FPS used in Fig. 4 for λ=647nm (red line), 568nm (green line), and 488nm (blue line).

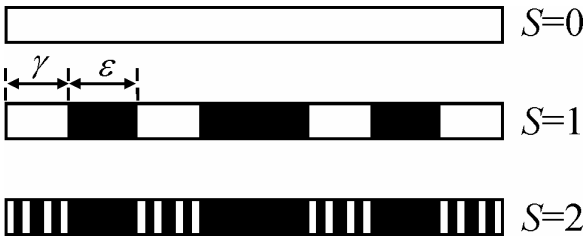

Figure 6. Schemes for the generation of a polyadic Cantor fractal set for N=4 up to S=2. γ is the scale factor and ε is the parameter that characterizes the lacunarity.

The construction of a typical polyadic Cantor fractal set with a specific lacunarity is shown in Fig. 6. The first step in the construction procedure consists in defining a straightline segment of unit length called initiator (stage S = 0). Next, at stage S = 1, the generator of the set is constructed by N (N = 4 in the figure) non-overlapping copies of the initiator each one with a scale $\gamma < 1$. At the following stages of construction of the set (S = 2, 3,...), the generation process is repeated over and over again for each segment in the previous stage.

To characterize the resulting Cantor set, as well as many other fractal structures, one of the most frequently-used descriptors is the fractal dimension, defined as

$$D = -\mathrm{In}(N)/\mathrm{In}(\gamma) \tag{4}$$

However, this parameter does not uniquely define the fractal. In fact, for the general case, it is necessary to introduce another parameter to specify the distribution of the N copies into the unit length segment. This parameter specifies the lacunarity of the resulting structure and it is essential to complete the characterization of the fractal because structures with different lacunarity can have the same fractal dimension. To define the lacunarity, we use the width of outermost gap in the first stage (see Fig. 6). This convention was also adopted in some previous papers dealing with Cantor fractals [3, 9, and 10]. It has been shown that regular fractal is a particular case of this general structure when the lacunarity ε, takes the following value:

$$\varepsilon_R = \frac{1 - N\gamma}{N - 1} \tag{5}$$

which is equivalent to impose that the bars and gaps have the same size at the initiator stage.

The LFPS here proposed has essentially the same structure of a lacunar FZP but instead of transparent rings the corresponding zones have been broken up into isolated circular holes randomly distributed (a photon sieve).

Now we investigate the focusing properties of a typical LFPS. To compare the performance of a LFPS with the associated lacunar FZP we used Eq. (3) to compute the axial irradiances provided by the pupil functions. The result is shown in Fig.7 together with the irradiances corresponding to analogous pupils constructed for S = 1. In order to observe the fractal behaviour of the irradiances for different stages of growth S, we have normalized the axial distance, z, to the principal focal length given by

$$f_S = \frac{a^2}{\lambda(2N-1)^S} \tag{6}$$

The self-similarity of the resulting axial irradiances can be clearly seen in Fig. 7(a). The dotted lines (S = 1) forms the envelope of the solid lines (S = 2). On the other hand, when the lacunar FZP is replaced by a LFPS the principal focus remains almost unaltered but all odd higher orders are highly reduced due to the smoothing effect that the holes produce on the azimuthal average of the effective pupil. This effect is obtained at the expense of the appearance of low intensity even orders, which by design are null in the case of azimuthally uniform FZP with $\varepsilon = \varepsilon_R$.

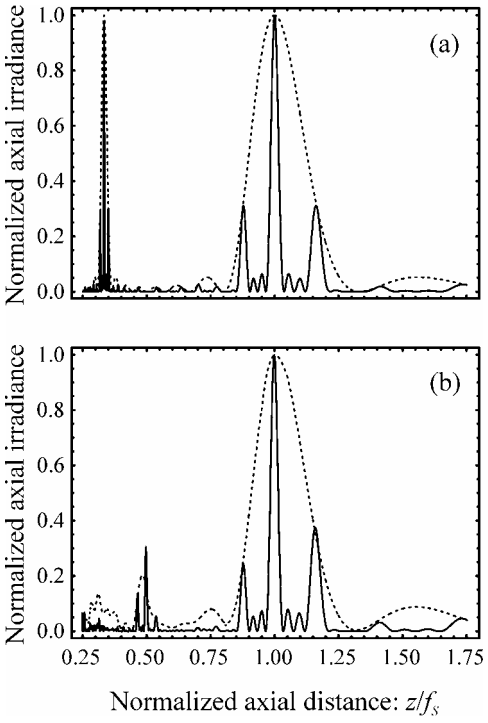

Figure 7. Normalized irradiance distribution along the optical axis produced by (a) FZP and (b) FPS shown in Fig. 2(a) and Fig. 2(b), respectively. The dotted lines represent the corresponding axial irradiances for *S*=1.

To show that the self-similar behavior provided by LFPS is retained even when the lacunarity paramter is varied, we have used twist plots [10]. These plots represent the axial irradiance as a function of the normalized axial distance and the lacunarity parameter ε . Fig. 8 shows twist plots for tetraedic (N = 4) LFPS S = 1 (a) and S = 2 (b). In these plots a linear gray level scale was used for the normalized axial irradiance.

The most noticeable feature of Fig. 8 is the self-similarity that can be observed between the plots corresponding to S = 1 and S = 2. In fact, the rescaled data at stage S = 1 forms an envelope for the data at S = 2, and both structures are self-similar for any value of ε. This result shows that the axial irradiance provided by polyadic LFPS has self-similar properties like to those reported for lacunar FZP [3]. However, from the focalization point of view LFPS are more efficient than lacunar FZP because the relative intensity of the main focus is much higher than the secondary foci.

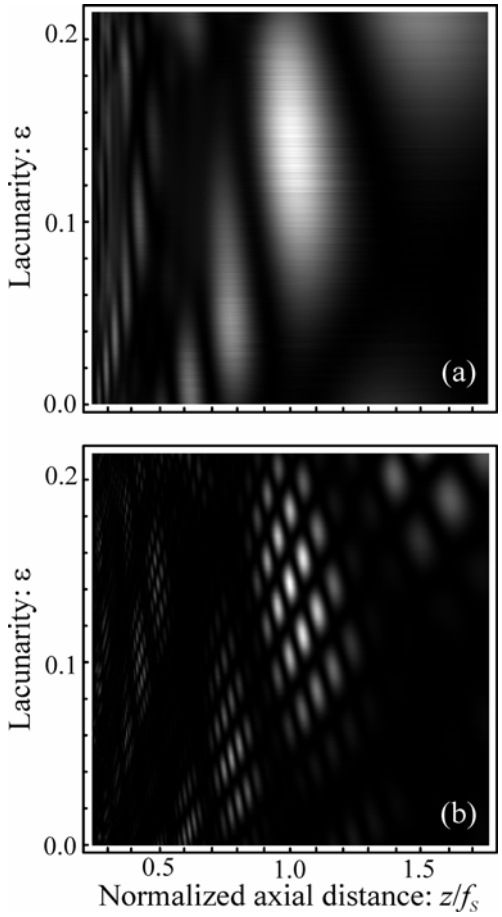

Figure 8. Gray-scale representation of the axial response plotted as a function of the normalized axial distance and the lacunarity of a LFPS (N=4, γ=1/7) for: (a) S=1, and (b) S=2.

3. Devil's lenses

Devil's lenses (DL) are new type of pure phase DOEs. DL is a kinoform element in which the surface relief is constructed using a function known as the *devil's staircase*. In this section we present the design and the focusing properties of this new design. We will call DL to any rotationally symmetric diffractive lens whose phase profile is designed from a devil's staircase function. A standard example of a devil's staircase is the Cantor function, which can be generated from any given Cantor set (CS). The first step in the CS construction procedure, consists in defining a straight-line segment of unit length called *initiator* (stage S=0). Next, at stage S=1, the *generator* of the set is constructed by dividing the segment into m equal parts of length $1/m$ and removing some of them. Then, this procedure is continued at the subsequent stages, S=2, 3. … Without loss of generality, let us consider the triadic CS shown in the upper part of Fig. 9(a). In this case m=3 and it is easy to see that, at stage S there are 2^S segments of length 3^{-S} with 2^S–1 disjoint gaps intervals $[p_{S,l}, q_{S,l}]$, with l=1,…, 2^S–1. Based on this fractal structure in this case the devil's staircase Cantor function $F_S(x)$ [11] can be defined in the interval [0,1] as a linear increasing function at the segments of the CS and it takes constant values at the gaps of the CS (Fig. 9).

From $F_S(x)$ we define the corresponding DL as a circularly symmetric DOE with a phase profile which follows the Cantor function at a given stage, S. At the gap regions defined by the Cantor set the phase shift is $-l2\pi$, with l=1, 2^S–1. Thus, the convergent DL transmittance is defined by

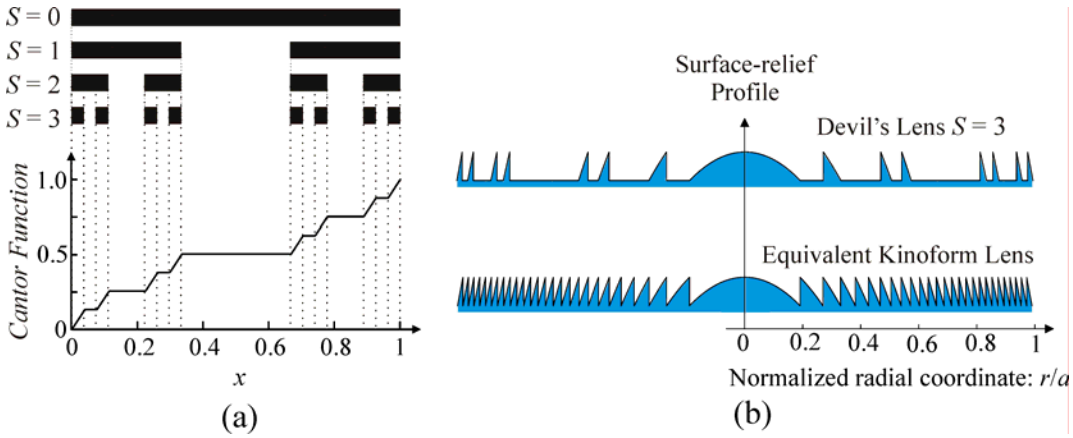

Figure 9. (a) Triadic Cantor set for S=1, S=2, and S=3. The structure for S=0 is the initiator and the one corresponding to S=1 is the generator. The Cantor function or Devil's staircase, $F_S(x)$, is shown under the corresponding Cantor set for S=3. (b) Convergent DL at stage of growth S=3 and the equivalent kinoform Fresnel lens.

$$q(\varsigma) = q_{DL}(\varsigma, S) = \exp\left[-\mathrm{i}\ 2^{s+1}\pi F_S(\varsigma)\right] \tag{7}$$

where

$$\varsigma = (r/a)^2 \tag{8}$$

is the normalized quadratic radial variable and a is the lens radius. Thus, the phase variation is quadratic in each zone of the lens. The surface-relief profile, $h(r)$, of the DL corresponding to the above phase function can be obtained from the relation [12]

$$h_{DL}(r) = \mathrm{mod}_{2\pi}\left\{-2^{s+1}\pi F_S\left(\frac{r^2}{a^2}\right)\right\}\frac{\lambda}{2\pi(n-1)} \tag{9}$$

where mod $_{2\pi}[\varphi(r)]$ is the phase function $\varphi(r)$ modulo 2π, n is the refractive index of the optical material used for constructing the lens, and λ is the wavelength of the light. The upper part of Fig. 9(b) shows the profile of a convergent DL generated using Eq. (9). For comparison we have depicted at the lower part of the same figure the profile corresponding to a conventional Fresnel kinoform lens of the same focal length. It is instructive to note that the DL can be understood as a conventional kinoform lens but with some missing phase zones.

Since we will consider DOEs whose minimum feature size is much greater than the wavelength of incident light we will use the scalar diffraction to evaluate their performance. In fact, we will show that even for the lower values of S the distinctive features of DLs are evident. Then, within that approximation, the irradiance at a given point in the diffraction pattern produced by a general rotationally invariant pupil with a transmittance $p(r_o)$ is given by

$$I(z,r) = \left(\frac{2\pi}{\lambda z}\right)^2 \left|\int_0^a p(r_o)\ \exp\left(-\mathrm{i}\frac{\pi}{\lambda z}r_o^2\right)\ \mathrm{J}_0\left(\frac{2\pi r_o r}{\lambda z}\right) r_o\,\mathrm{d}r_o\right|^2 \tag{10}$$

where z is the axial distance from the pupil plane, r has its origin at the optical axis, and λ is the wavelength of the incident monochromatic plane wave. If the pupil transmittance is defined in terms of the normalized variable in Eq. (8), the irradiance can be expressed as the Hankel transform of the pupil function,

$$I(u,v) = 4\pi^2 u^2 \left|\int_0^1 q(\varsigma)\ \exp(-\mathrm{i}2\pi u\varsigma)\ \mathrm{J}_0\left(4\pi\sqrt{\varsigma}uv\right)\ \mathrm{d}\varsigma\right|^2 \tag{11}$$

where $q(\varsigma)=p(r_o)$. In Eq. (11), $u=a^2/2\lambda z$ and $v=r/a$ are the reduced axial and transverse coordinates, respectively. If we focus our attention to the values the irradiance takes along the optical axis, then $v=0$, and Eq. (11) reads

$$I_0(u) = 4\pi^2 u^2 \left| \int_0^1 q(\varsigma) \exp(-i 2\pi u \varsigma) \, d\varsigma \right|^2 \tag{12}$$

Thus, the axial irradiance can be expressed in terms of the Fourier transform of the mapped pupil function $q(\varsigma)$. Using Eq. (7) for the transmittance corresponding to a DL and taking into account that one of the features of self-similar structures is that the dimensionality of the structure appears in its power spectrum [1], then Eq. (12) predicts that a DL will produce an irradiance along the optical axis with a fractal profile that resembles the structure of the DL itself. To show this fact explicitly, the axial irradiance of the DL computed for different stages of growth S is shown in Fig. 10. The irradiance of the associated kinoform Fresnel lens is shown in the same figure for comparison. Note that the scale in the axial coordinate for each value of S is different. It can be seen that the axial position of the focus of the Fresnel kinoform lens and the central lobe of the DL focus both coincide at the normalized distance $u=3^S$. Thus, from the change of variables adopted in Eq. (11) the focal length of the DL can be expressed as

$$f_S = \frac{a^2}{2\lambda 3^S} \tag{13}$$

As expected, the axial response for the DL exhibits a single major focus and a number of subsidiary focal points surrounding it, producing a the focus region with a characteristic fractal profile. In fact, the three patterns in the upper part of Fig. 10 are self-similar, i.e., as S becomes larger an increasing number of zeros and maxima are encountered, which are scale invariant over dilations of factor $\gamma=3$. The axial intensity distributions corresponding to the ZPs of low level involve the curves of the upper ones. This focalization behavior, which is here demonstrated that DLs satisfy, is, in fact, an exclusive feature of FZPs and it was called *the axial scale property* [1]. Interestingly the main focus of the DLs presents a certain degree of axial superresolution. This effect is particularly evident from the comparisson of the upper and lower parts in Fig.10 for the irradiances corresponding to $S=2$ and $S=3$. Of particular interest are the intensities at transverse planes corresponding to the different maxima and minima of the axial irradiance. These are depicted in Fig. 11 together with their relative intensities. Note that the predicted minima are characterized by a concentric doughnut form.

When using broadband illumination the monochromatic irradiances provided by the diffractive lenses regarded so far are affected by chromatic dispersion, as shown in Fig. 12. In the case of DLs the subsidiary foci can beconsidered as an extended depth of focus for each wavelength and, as can be seen, they partially overlap with the other ones creating an overall extended depth of focus, which should be less sensitive to the chromatic aberration than the conventional Fresnel kinoform lens.

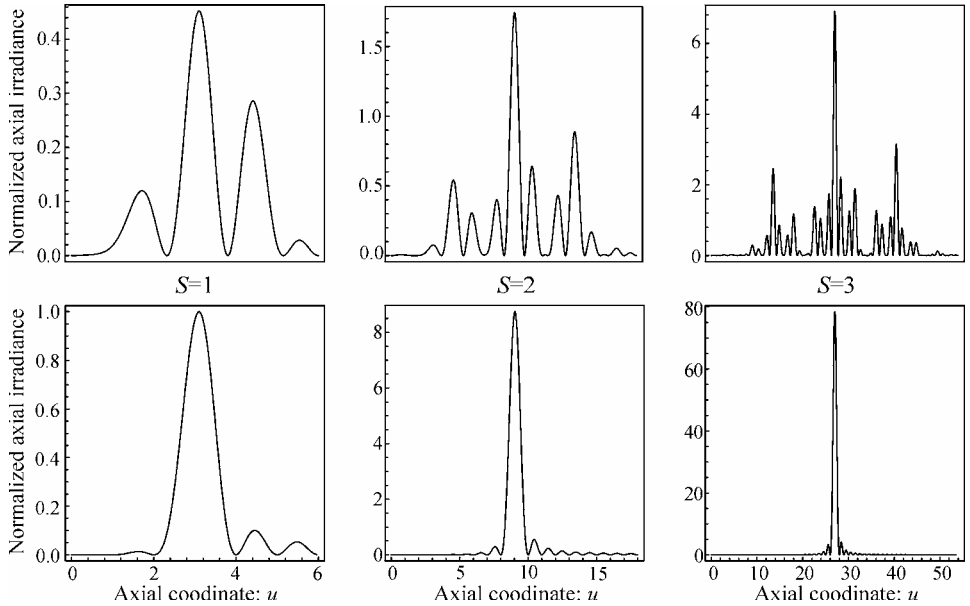

Figure 10. Normalized irradiance vs. the axial coordinate u obtained for aDL at three stages of growth (upper part) and for its associated Fresnel kinoform lens (lower part).

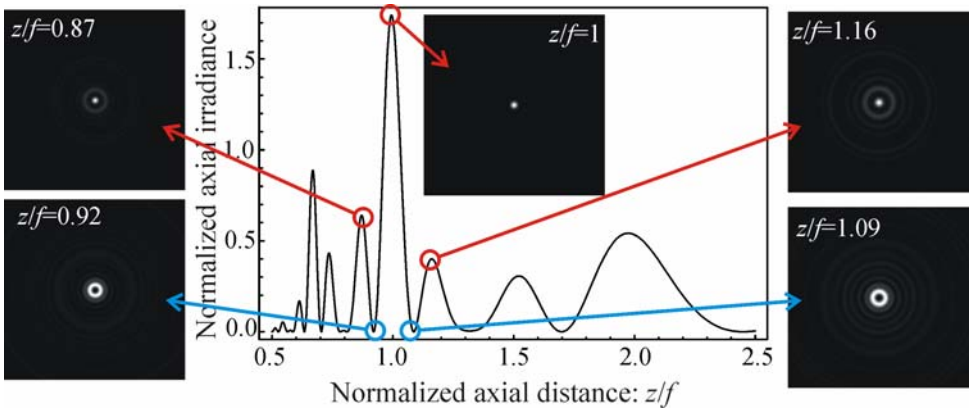

Figure 11. Transverse diffraction patterns around the principal focus of a DL with S=2. The normalized axial distance is given by $z/f_2=3^2/u$.

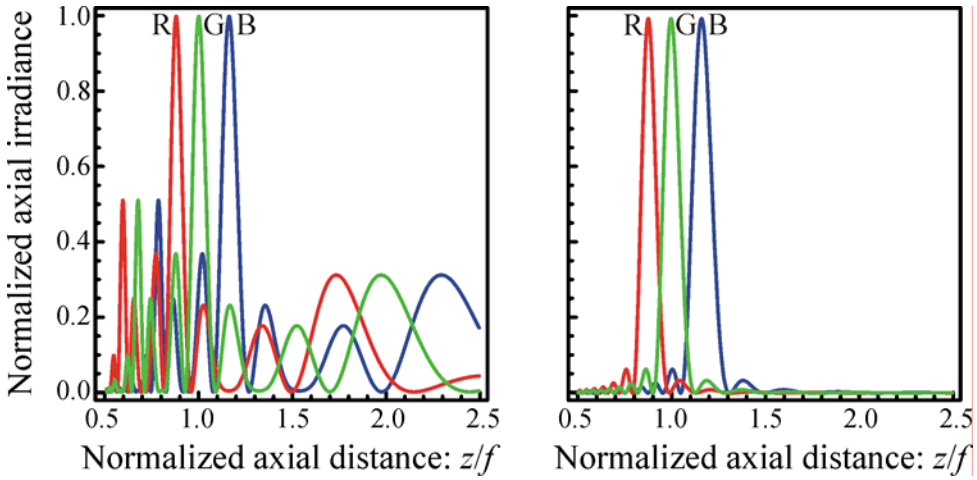

Figure 12. Normalized irradiance vs. the axial coordinate u obtained for a DL (left) and for its associated Fresnel kinoform lens for three wavelengths R=650 nm; G=550 nm; and B=480 nm. In all cases S=2.

4. Conclusions

The focusing and imaging properties of PFS have been revised. We demonstrated that a FPS has an extended depth of field and a reduced chromatic aberration compared with a Fresnel zone plate of the same focal length. The distribution of the holes is a degree of freedom that you can be exploited to perform apodization, particularly to nearly suppress the higher order foci. Another advantage of FPS over the FZP arises from the fabrication point of view: the FPS can be constructed in a single structure without any supporting substrate. Besides FPS can be also employed as a versatile focusing device in other regions of the electromagnetic spectrum, such as microwaves and X-rays or even with slow neutrons, in which graded amplitude pupils are difficult or even impossible to construct.

On the other hand, a new type of pure phase DOEs, coined “devil’s lenses”, has been introduced. To avoid the absorption losses that characterize amplitude fractal zone plates and to improve their diffraction efficiency the phase function for a typical DL has a quadratic-fractal blazed profile. It is shown that the distribution of the surface grooves of these fractal lenses is obtained through the “devil’s staircase” or Cantor function. When highly monochromatic sources are available the irradiance along the optical axis provided by a DL presents a single fractal focus with a characteristic fractal profile which results in a certain degree of axial superresolution for the main axial lobe. The minima appearing side by side around this lobe present transverse doughnut modes. The potential uses of DLs are numerous in applications where a high depth of field is desirable but where the illumination

sources are wideband. These applications cover different scientific and thecnological areas that use diffractive optics ranging from soft X-ray microscopy to THz imaging.

Aknowledgements

This research has been supported by the follwing grants:
-DPI2008-02953, Plan Nacional I+D+I, Ministerio de Ciencia e Innovación, Spain.
-GV/2007/239, Conselleria de Empresa, Universitat i Ciència, Generalitat Valenciana, Spain,
- PAID-05-07 and PAID-06-08 , Universidad Politécnica de Valencia, Spain.

References

1. G. Saavedra, W. D. Furlan, and J. A. Monsoriu, "Fractal zone plates," *Opt. Lett*. **28,** 971-973 (2003).
2. W.D. Furlan, G. Saavedra, and J.A. Monsoriu, "Fractal zone plates produce axial irradiance with fractal profile," *Opt. & Photon. News,* **14**(12), 31 (2003).
3. J.A. Monsoriu, G. Saavedra, and W. D. Furlan, "Fractal zone plates with variable lacunarity," *Opt. Express* **12**, 4227-4234 (2004).
4. J.A. Monsoriu, W.D. Furlan, and G. Saavedra, "Focusing light with fractal zone plates," *Resent Res. Devel. Optics* **5**, 65-79 (2005).
5. F. Giménez, J.A. Monsoriu, W.D. Furlan, and A. Pons, "Fractal photon sieve," *Opt. Express* **13**, 11958-11963 (2006).
6. F. Giménez, W.D. Furlan, and J.A. Monsoriu, "Lacunar fractal photon sieve," *Opt. Commun.* **277**, 1-4 (2007).
7. J.A. Monsoriu,W.D. Furlan, G. Saavedra, and F. Giménez, "Devil's lenses," *Optics Express*, **15**, 13858-13864 (2007).
8. L. Kipp, M. Skibowski, R. L. Johnson, R. Berndt, R. Adelung, S. Harm, and R. Seemann, "Sharper images by focusing soft x-rays with photon sieves," *Nature* **414**, 184-188 (2001).
9. D.L. Jaggard and A.D. Jaggard, "Polyadic Cantor superlattices with variable lacunarity," *Opt. Lett.* **22**, 145-149 (1997).
10. A.D. Jaggard and D.L. Jaggard, "Cantor ring diffractals," *Opt. Commun*. **158**, 141-148 (1998).
11. D. R. Chalice, "A characterizationof the Cantor function," *Amer. Math. Monthly* **98**, 255-258 (1991).
12. Y. Han, L. N. Hazra, and C. A. Delisle, "Exact surface-relief profile of a kinoform lens from its phase function," *J. Opt. Soc. Am. A* **12**, 524-529 (1995).